UNIVERSITY OF OKLAHOMA

GRADUATE COLLEGE

QUANTIFYING SPATIAL-TEMPORAL STABILITY TO DROUGHT IN A SEMI-ARID SHORTGRASS PRAIRIE ECOSYSTEM

A THESIS

SUBMITTED TO THE GRADUATE FACULTY

in partial fulfillment of the requirements for the

Degree of

MASTER OF SCIENCE

By

ERIC ALLEN
Norman, Oklahoma
2022

QUANTIFYING SPATIAL-TEMPORAL STABILITY TO DROUGHT IN A SEMI-ARID SHORTGRASS PRAIRIE ECOSYSTEM

A THESIS APPROVED FOR THE
DEPARTMENT OF MICROBIOLOGY AND PLANT BIOLOGY

BY THE COMMITTEE CONSISTING OF

Dr. Lara Souza, Chair

Dr. Heather McCarthy

Dr. Xiangming Xiao

Acknowledgments
I would like to thank my fiancée, Amy Banka, as well as my family for their support throughout the past two and a half years. I would like to recognize my advisor, Dr. Lara Souza for her guidance and assistance with this research, and with all of her help navigating the curveballs COVID-19 threw at us. I would also like to acknowledge the contributions and suggestions of my committee and lab members, as well as Dr. Claire Curry and Dr. Kirsten De Beurs for their advice regarding statistical methods and analysis.

Table of Contents

List of Tables and Figures

Abstract

Drought is known to cause negative ecological impacts in grasslands, with areas prone to drought expected to experience increases in both severity and frequency in the coming years. Cimarron County, Oklahoma is located at the westernmost extent of the Oklahoma panhandle and has a history of intense drought events, including those of the Dust Bowl era. Since 2005, there have been repeated droughts in the county, including a single event lasting from 2011-2015. We analyzed remote sensing data to understand the spatial and temporal stability of grassland structure (Enhanced Vegetation Index) and function (Gross Primary Productivity) within Cimarron County with reference to drought. Drought was quantified using the Standardized Precipitation Index, derived from a remotely sensed precipitation dataset. Stability was quantified by applying the BFAST (Breaks for Additive Season and Trend) algorithm to determine structural breaks within each metric's time series, and by calculating the coefficient of variation for each pixel across the county. Temporal data show that while these grasslands display characteristics of low stability at the onset of drought, they exhibit consistent positive trends in EVI and GPP following each drought event, recovering, and sometimes eclipsing their pre-drought levels. Spatial data indicate high spatial heterogeneity in EVI and GPP variability across the county, and a relatively low but significant correlation with drought variability. These analyses suggest while drought has a significant effect on grassland stability, there are likely many other drivers, and while the onset of drought greatly effects grassland structure and function, they are consistently able to rebound and regain their pre-drought levels. Although these grasslands are impacted by drought, their ability to recover is

rapid. Likely, plant composition or drought events are taking place during times of dormancy and mediating these responses, when plants may be less affected.

Keywords: Drought, Remote sensing, Spatial-Temporal, Grasslands, Stability

1. Introduction

1.1 Remote sensing and ecosystem stability

Drought is known to cause negative ecological impacts including reduction in vegetation structure and function (Knapp et al., 2008; Weltzin et al., 2003; Zhang et al., 2016), with areas prone to drought expected to experience increases in both severity and frequency, including possible shifts in intra-annual precipitation (Zhou et al., 2019, Knapp et al., 2020). Shifts in intra-annual variation in precipitation can be as impactful on ecosystems as annual drought events, potentially causing shifts in vegetation composition such as the ratio of warm (C_4) to cool (C_3) season graminoid dominance in grassland ecosystems. Due to these projected increases in intra-annual variability in precipitation, acquiring a deeper understanding of ecological system responses to the effects of drought may be imperative for future assessment and mitigation. Oscillations in vegetation biomass within an ecosystem can be indicators of ecological responses to perturbations and exploring these variations in respect to drought may give us a greater understanding of their influences on ecological systems (Ma, 2017).

Understanding ecosystem stability to drought has been a thrust in ecological studies (Tillman, 2006), and more recently addressed with remote sensing products (Keersmacker et al., 2014). Ecological stability is generally defined as the ability of an ecosystem to resist and/or rapidly recover from perturbations such as drought (Rutledge, 1976). Intense drought can heavily affect grasslands, with one study noting short-term decreases in grassland biomass by almost 50% during intense drought over the course of

one year (Tilman, 1992). However, vegetation biodiversity can contribute towards promoting grassland resistance and recovery to drought events (Tillman, 1994). Remote sensing data is valuable for studying drought across landscapes due to its reliability and global coverage (Goward et al., 2006). Vegetation indices, such as EVI, are derived from remote sensing data and are designed to be indicative of several biophysical parameters of vegetation. They are calculated using values derived from the spectral reflectance of two or more bands along the electromagnetic spectrum, and have been implemented as indicators of vegetation biomass, structure, and vigor (Ji, 2006). Satellite derived Gross Primary Productivity (GPP) datasets are commonly used to study vegetation function at large scales, and can give insight into changes in vegetation functioning over time (Kuhn, 2020)

The accurate use of remote sensing data to estimate ground level productivity has been addressed (Tebbs, et. al, 2017) finding strong relationships between remotely sensed vegetation productivity and ground level estimates, allowing for the mapping of vegetation productivity from local to regional scales. Further, drought has shown measurable effects within remote sensing measurements of vegetation structure and function (Vicca, 2016; Zhang, 2021). With this known, analyzing the fluctuations of these data, both spatially and temporally, may be useful in understanding how regions are positively and negatively responding to drought.

1.2 Grassland stability and drought

Studies have found the presence of long-term oscillations and decreases in aboveground net primary productivity of grasslands following severe drought (Haddad, 2002; Chong, 2021). These data indicate grassland function can be affected by disturbances such as drought long after an individual event has concluded. With remote sensing data, quantifying the ecological impact of drought on the stability of ecosystem structure and function could have great implications for land management (Vogel, 2012; Reinermann, 2020). Remote sensing can allow monitoring but also forecasting of ecological responses to drought (Iftikhar, 2016).

The utilization of remote sensing has allowed for extensive data collection and analysis, and with the application of high spatial-temporal resolution imagery, time series analysis has been key in studying ecosystem responses over time (Southworth, 2021).
Remote sensing has been applied to study resilience of vegetation to drought and the stability of ecosystems across large areas over the course of known disturbances (Feng, 2021, White, 2020), with one study finding low stability of semi-arid grasslands to drought worldwide (Keersmaecker et al., 2015).

Shifts in seasonal precipitation can have strong impacts on grassland ecosystems and have been found to lead to shifts in grassland composition, such as increases in the ratio of C_3 to C_4 grasses due to the occurrence of drought predominantly during winter months rather than the growing season (Witwicki et al., 2016; Knapp et al., 2020). Increases in intra-annual variation of precipitation can be as impactful on ecosystems as annual events, and it has been noted that these intra-annual variations can cause shifts can occur

in vegetation composition due to differences in phenology between vegetation types (Shaw et al., 2021), and intra-seasonal variability in rainfall patterns may contribute to a large variation in annual ANPP (Frank & Inouye 1994; Knapp & Smith 2001).

Grasslands are the largest terrestrial ecosystem on Earth, ubiquitously distributed in the landscape across space and time (Ali, 2016), and provide numerous ecosystem services and economic products (Wang, 2019). Grasslands are important sources of biodiversity and productivity, while facilitating ecosystem functions (Munson, 2017). For instance, grasslands can serve as reliable carbon sinks, though drought can significantly influence interannual variation in terrestrial carbon dynamics and overall sequestration, with grasslands often shifting between carbon sources in drought years and carbon sinks in other years (Zhang, 2011).

This study applies remote sensing approaches to assess vegetation structure and productivity responses to drought over a period of 16 years (2005-2020), in which four drought events occurred, with the last still ongoing as of December 2020. The first three droughts during this timeframe were each more intense than the last, and it is unknown as what the extent of this fourth drought will be. The objective of this study is to understand how the structure and function of grasslands across Cimarron County, Oklahoma have been affected by drought, and how they are responding over time within the context of stability (e.g., resistance, recovery). The grasslands of Cimarron County, Oklahoma are of relevance, as much of their area is used for cattle grazing, with Cimarron County being the third largest cattle producing county in Oklahoma (USDA, 2019). Grassland

senescence and possible degradation may become an issue if these grazing lands are to continue to be used at their current rate during times of increased drought. Specifically, we asked 1) How does temporal variation in drought events affect vegetation structure and function across time? 2) How do vegetation structure, function, and stability vary across space.

2. Materials and methods

2.1 Study Area

Cimarron County, Oklahoma is located at the far western terminus of the Oklahoma panhandle, bordered by the U.S. states of Kansas, Colorado, New Mexico, and Texas (Figure 1) (Vadjunec, et al., 2021). It is situated in the High Plains and Southwestern Tablelands of Oklahoma, with shortgrass prairie being the dominant grassland ecosystem (Hoagland, 2000). The dominant grasses in the shortgrass prairie are buffalo grass (*Buchloe dactyloides*) and blue gramma (*Bouteloua gracilis*). These species are both drought tolerant perennial C_4 grasses and make up approximately 70-90% of the shortgrass prairie composition by biomass (Lauenroth, 2008).

Cimarron County has a cold semi-arid climate (Köppen *BSk*) with cold winters and hot, dry summers. The area is prone to frequent and severe drought with an average precipitation of approximately 38-51 centimeters per year, with most falling May-August. Temperatures in the county range from an average high of 93 degrees Fahrenheit in July to an average low of 19 degrees Fahrenheit in January (Oklahoma Climatological

Survey). Figure 2 shows monthly mean, minimum, and maximum precipitation and temperature for Boise City, Oklahoma, located in central Cimarron County.

The years 2005-2020 were chosen as the time frame for this study, as four drought events occur during this span, including Oklahoma's most intense and extensive drought since 1964 (Mesonet). We were also unable to gather data prior to 2005 due to historical limitations in our datasets.

2.2 Quantifying grassland cover

The Cropland Data Layer (CDL) is an annual landcover-type specific map of the United States created by the United States Department of Agriculture (USDA). The categories include landcover types such as grasslands, shrublands, evergreen forests, and many different crop types, with an accuracy of approximately 85-90% when quantifying grassland/pasture landcover (Lark, et al., 2017). We applied the CDL in order to isolate all grasslands within the borders of Cimarron County. As the extent of each CDL category changes year to year (Figure 3), SPI, EVI and GPP data were cropped to their respective year's CDL grassland map. Once the grassland pixels were converted from grasslands to other LULC types, they were never re-introduced into the dataset, so it is unlikely grassland conversion had any effect on the observed drought responses (Table 1).

2.3 Quantifying vegetation structure and productivity

The Enhanced Vegetation Index is a vegetation index calculated with the combination of blue, red, and near infra-red wavelengths and was developed to detect canopy greenness, while limiting the effects of atmospheric conditions such as clouds, aerosols, and general background noise (Masek, 2006). We chose EVI over other vegetation indices because of this ability to limit atmospheric effects, as the study area is prone to dust storms during times of drought. The application of EVI will likely lessen the noise created by dust suspended in the atmosphere.

We computed EVI of Cimarron County's grasslands from 2005-2020 using an EVI dataset within Google Earth Engine's data catalog to determine vegetation structure responses to drought (Masek, 2006). This EVI dataset provides values every eight days at 30-meter spatial resolution, which we then averaged seasonally into three-month time periods to account for vegetation response lag (Hua, et al., 2019).

$$EVI = 2.5 * ((NIR - Red) / (NIR + 6 * Red - 7.5 * Blue + 1))$$

EVI formula

To determine responses of grassland function to drought, we quantified Gross Primary Productivity (GPP) of Cimarron County's grasslands from 2005-2020 using a Landsat-derived GPP dataset provided in Google Earth Engine's data catalog (Robinson, 2018). This dataset provides GPP values once every 16 days at 30-meter spatial resolution, which we then averaged seasonally into three-month time periods to account for vegetation response lag.

2.4 Determination of drought

Drought indices are calculations used to determine the presence and intensity of drought in an area. The Standardized Precipitation Index (SPI) is a drought index that compares precipitation in a specified area to precipitation averages from long-term records, typically 30-50 years. SPI has been found to perform well when quantifying drought across large geographical areas in diverse natural systems, and when quantifying various types of drought at a range of timescales (Guenang, et al., 2014; Wang, et al., 2017).

We gathered 12-month SPI data for the study area by accessing a SPI dataset through Google Earth Engine's data repository (Abatzoglou, et al., 2012). We used SPI data from 2005-2020 to quantify the presence and severity of the drought events occurring across this timeframe. SPI values at or below -1 indicate precipitation at least one standard deviation from the norm and are typically used as a threshold for the onset of drought (Figure 4) (Keyentash, 2018). The same method is also used to determine pluvial events with precipitation at or above a SPI value of one.

There were four dates with missing values for SPI, which were filled using linear interpolation. As our SPI data had a spatial resolution of approximately 4000 meters, it was necessary to upscale in order to match out EVI and GPP datasets at 30 meters (Figure 5).

2.5 Time series processing and analysis

When extracting time-series data from the rasters, median values were taken for each season to limit the effects of cropland outliers on the grassland data. These cropland EVI and GPP values could affect the overall grassland values, especially during times of drought due to the effects of irrigated and highly productive crops such as corn, compared to relatively low productivity grasslands.

We used SPI rather than raw precipitation data because we wanted an accurate indicator of the beginning and end of each drought and pluvial event. This was essential so we could cross-reference timing of SPI values with corresponding breakpoints. SPI can be thought of as the number of standard deviations by which a normally distributed random variable deviates from its long-term mean (Guenang, et al. 2014), therefore it is mostly unaffected by seasonal variation. In order to accurately compare drought with vegetation structure and function, we needed to apply a moving average to each time series, so SPI, EVI, and GPP time series were in the same seasonally adjusted format. This removal of seasonal variation was done using the "ma" function in the "Forecast" package in R (Hyndman, 2021). After this was implemented, we calculated the correlation coefficients using the "spearman" method of the "cor.test" function in the "Stats" package in R (R Core Team, 2013). This was performed to find overall correlations between the smoothed times series.

2.6 Quantifying Temporal Stability

We chose to quantify temporal stability by assessing abrupt changes within each time series using the "BFAST" function from the "BFAST" package in R (Verbesselt, 2010).

Breaks for additive season and trend, or BFAST has been successfully used to detect drought disturbances in time series data, as (Gao et. al, 2021) found abrupt changes, or "breakpoints" located along multiple vegetation index time series, where previously known sudden changes in the data occurred. If breakpoints in EVI and GPP time series happen at the same time as those in the SPI time series, it may indicate variability or abrupt changes in precipitation have a significant effect on the temporal stability of EVI and GPP.

Verbesselt, 2012 identified "stable" periods as those between breakpoints, as they represent time periods of "normal" variation, thus breakpoints identify a specific point of temporal instability. These points of instability may signal vulnerability to similar climate events in the future.

2.7 Quantifying Spatial Stability

We created rasters using median values for each three-month season (*Jan-Mar: Winter, Apr-Jun: Spring, Jul-Sep: Summer, Oct-Dec: Fall*) for each year in order to minimize lag effects between SPI fluctuations and EVI/GPP responses, as well as limit the number of rasters, as each raster contains approximately eight million data points. The three-month seasons of spring and summer paired well with the growing season in Cimarron County, which lasts approximately 172 days (Oklahoma Climatological Survey).

The BFAST algorithm was not performed on the spatial data due to variations in the spatial extent of grasslands from year to year. Grassland area changes every year due to

annual updates in the CDL and would have caused unequal values in the amount of data points per pixel area because grassland areas converted from or transitioned to other land cover types would then become N/A values. Interpolation techniques to fill these N/A values were not an option, as the focus of this study is grasslands specifically. Due to these missing values, some locations may have generated all 64 data points, whereas other areas may have had a few as four data points (one year), before they were converted or changed to land cover other than grasslands.

In lieu of the BFAST algorithm, coefficient of variation (CV) was calculated for the entire raster stack of 64 images using the "cv" function in the R package "Raster" (Hijmans & van Etten, 2012), to determine areas within the county that underwent the largest amount of variation, and thus possessed the least amount of stability over the full timeframe. CV was also calculated seasonally to see which areas in each season grasslands showed the most variation in EVI, GPP, and SPI respectively.

To understand the relationships between variations in SPI, EVI, and GPP, we extracted CV values from each variable's raster stack and ran linear regressions on the CV for each season's raster stack, as well as the full timeframe.

3. Results

3.1 Drought and pluvial events

We documented turbulence within precipitation patterns from 2005-2020, including five distinct drought events and six pluvial events based on SPI (Figure 6).

There were 33 seasons with below average and 27 seasons with above average precipitation according to SPI. The season with the lowest average SPI values was Fall (-0.3109211) while the season with the highest was Spring (-0.026875). The longest time periods of continuous below and above average precipitation are 17 and 19 seasons respectively. Summer and Spring had the most occurrences of drought (Table 2), though season with the most intense droughts and lowest average SPI was Fall (Tables 3 & 4).

3.2 Relationship between SPI and EVI, GPP time series and rasters

We found strong positive spearman correlation values between EVI, GPP, and SPI time series: SPI~EVI: r^2= 0.73, p = < 2.2e-16; SPI~GPP: r^2=0.81, p = < 2.2e-16; EVI~GPP: r^2= 0.73, p = < 2.2e-16). These data may indicate similar trends between drought, vegetation structure, and vegetation function throughout the course of an extended timeframe containing multiple drought and pluvial periods. Linear regression models run between data extracted from each variables' raster stack show relatively weak but significant relationships, with SPI-EVI and SPI-GPP models displaying the strongest correlations (Table 5).

3.3 Quantification of temporal stability

BFAST analysis shows three breakpoints for both EVI and GPP, with SPI exhibiting four breakpoints. Generally, the three breakpoints for EVI and GPP coincide with the onset of the 2008 drought, onset of the 2011 drought, and the onset of the 2016 pluvial period (Figure 7). The SPI time series breakpoints also coincide with these events, with the addition of a fourth breakpoint in 2013, which appears to coincide with the

lowest SPI in the 2011-2015 drought period. These data indicate stable periods of EVI and GPP seem to last as long those of SPI, apart from the third SPI breakpoint.

3.4 Quantification of spatial-temporal stability

There was substantial seasonal variation in EVI and GPP according to coefficient of variation data (Figure 8); SPI values showed the highest variability (117.08), with EVI (40.88) and GPP (87.97) showing much lower variation across space and time. Further, SPI showed a relatively low range of variation across seasons (12.45) while GPP varied the greatest (19.05). Spring generally showed the most variation across time, followed by winter, summer, and fall (Table 6).

Overall, SPI had a considerably larger CV than both EVI and GPP, which may be a partially product of the generally high variability within precipitation patterns for the region. Each metric's CV map is shown in figure 9, highlighting areas of high and low variability, with those values presented in figure 10 to display their distribution. For better visualization, outliers were removed by calculating the inter-quartile range and multiplying it by 1.5. From there, we added this value to the third quartile and subtracted from the first quartile, excluding values outside of those ranges. There is a weak but significant relationship between SPIcv and both EVIcv and GPPcv. SPIcv explained less than 1% of the variation in EVIcv and less than 4% of GPPcv (Table 7).

4. Discussion

We documented synchronicity between drought & pluvial events (SPI), and vegetation structure (EVI) and function (GPP) over time. However, during the longest and most

intense drought events/periods, SPI exhibited a fourth breakpoint, whereas grassland EVI and GPP continued on a positive recovery trend after the onset of this drought event. There were modest but significant positive relationships between temporal variation in drought and variation in grassland structure and function.

The lack of a fourth break within both the EVI and GPP time series may indicate temporal stability to drought within the grasslands, as the variation within their time series was not significantly altered between the second and fourth SPI breakpoint, even as SPI continued to decrease (increase in intensity) during this time period. Van Ruijven & Berendse, 2010 and Wilcox et al., 2020 noted similar patterns of rapid recovery of semi-arid grasslands to extreme drought.

While the grasslands in this study were strongly affected by drought in general as indicated by the steep declines of EVI and GPP with the onset of each drought period, they also present steady recovery responses even to large fluctuations in inter- and intra-annual precipitation. The similarity between the timing of each EVI and GPP break indicates the BFAST model and other similar analyses may be very useful in automatically identifying the timing of drought driven disturbances within grassland ecosystems (Vicca et al., 2016).

Although in this study, it is unknown specifically which characteristics of this shortgrass prairie ecosystem drive its ability to undertake these steady positive responses, one mechanism may be driven by shifts in plant composition as a process which promotes

rapid grassland recovery from drought events (Wilcox, 2020). Another aspect is likely the inherent drought tolerance of C_4 grasses that dominate the shortgrass prairie (Knapp, 2020). Chong, et al., 2021 subjected semi-arid grassland plots to multiyear extreme droughts, finding full recovery to pre-drought within two years following the drought, noting mediation of negative effects by functional group composition shifts (decreases in forbs and increases in drought resistant grasses during extended drought treatments). These factors might explain why EVI and GPP did not show a breakpoint aligning with the third SPI breakpoint, and instead continued in a positive progression whereas SPI continued decreasing three more years until 2016.

Shifts in drought seasonality can be another contributing factor to rapid grassland recovery to intra-annual precipitation variability. The strong positive responses of grassland structure and function could be partially explained by the fact that fall (Oct.-Dec.) had the lowest overall SPI. If the most intense droughts occurred during periods of time in which the vegetation has gone dormant, there may be less of an effect on the vegetation versus a drought occurring through the growing season. This contrasts with existing literature, as past studies have found spring droughts to show the least effect on C_4 grasslands, and cooler, late season (fall/winter) droughts to have the greatest negative effect on overall C_4 grassland productivity (Arredondo, 2016; Churchill, 2022). Mixed (C_3/C_4) grasslands show increases in C_3 productivity at times when precipitation is decoupled from temperature, such as cool-season drought. Knapp et al 2020 found cool-season droughts create conditions allowing C_3 grasses to proliferate and compensate for losses in C_4 productivity, even across multi-year droughts.

At the start of the 2011-2015 drought, the most intense parts of the drought occurred in the cooler fall and winter seasons, while the grasses remained dormant. This may partially explain how grassland structure and productivity were able to respond positively throughout the rest of the period when drought was relatively less intense.

It is unlikely these responses were driven by short-term physiological responses of grassland vegetation. What is more likely are the occurrence of shifts in vegetation composition within the grasslands, allowing for positive short and long-term responses to drought. Wilcox, 2020 found grassland productivity to have a strong decrease during drought, while also exhibiting quick positive responses following drought events. It was determined this response was due to subdominant grass species compensating for declines in dominant species productivity, a process supported by other grassland studies (Mariote et al., 2013). Overall, shifts in composition can contribute towards recovery either by: (1) dominant species recovering quickly especially if drought doesn't co-occur with its time of activity or (2) subdominant species recovering quickly given that drought may not co-occur with its phenology.

Due to the considerable cattle and pastureland presence within the county, it is possible grazing may have also impacted the spatial and temporal results. Arredondo, 2016 found C_4 dominated grassland sites that experience a high degree of disturbance such as overgrazing, the dominant species was replaced by commonly subordinate C_4 perennial grasses, annual C_3 grasses, and C_3 forbs, forming diverse mixed grassland communities

with various functional characteristics. While intense grazing can negatively impact and drive grassland degradation (Fang and Wu, 2022), moderate grazing may promote grassland stability over time, increasing resilience and diversity, even compared to un-grazed grasslands (Souther, 2020).

The spatial results agree with existing literature suggesting grasslands possess a wide variation of buffering responses to disturbances such as drought. Differences in factors including plant traits and soil fertility may mediate these drought responses, allowing for high spatial variation within a system (Luo et al., 2021), suggesting most native grasslands are likely to contain a high diversity of drought tolerance. These characteristics along with a high diversity of drought tolerance across the grasslands landscape may bring about the observed heterogeneity in spatial stability (Craine, et al., 2012).

The coefficient of variation for both EVI and GPP show noticeably more locality and heterogeneity across the county than SPIcv. So much so, that geographic and topographic features such as rivers and canyons can be made out visually, possibly due to the patterns of variation these features may give rise to. The weak relationship between drought and grassland structure and function is likely due to the fact that over the course of 16 years, SPI had essentially equal variation across the county, limiting the strength of the correlations with the much greater spatial heterogeneity of EVI and GPP variation. There is also certainly land management occurring throughout the grasslands, which may be mitigating some of the direct effects of drought on vegetation structure and function.

BFAST analysis appears to be useful in detecting drought-associated disturbances across time, pairing well with SPI values indicating drought and pluvial periods. BFAST was also successful in detecting EVI and GPP responses to drought, indicating the onset of drought has a substantial effect on vegetation structure and function within grasslands, a phenomenon seen in and corroborated by other studies (Hahn, 2021; Mackie, 2018)

Future directions could include applying BFAST to more extended temporal datasets to detect more structural breaks and patterns within time series. With an increase in temporal data, BFAST results could potentially be integrated into predictive models for forecasting long-term grassland stability to drought.

6. Conclusions

The grasslands of Cimarron County, Oklahoma experienced a wide range of precipitation variability from 2005-2020, displaying negative effects at the onset of drought, but notably exhibiting steady responses in the following seasons and years. As our climate changes and droughts increase in quantity, intensity, and extent it may be imperative to understand the dynamics of grassland structure (dominant vs. subdominant species responses) and productivity in respect to environmental disturbances. This knowledge should assist in protecting grasslands from degradation, as well as determining how these fluctuations might affect the climate as a whole. The findings of this research may aid in understanding grassland responses to potential frequent and intense droughts in the

coming years and give insight into factors to be considered when managing grasslands to increase their stability under the effects of drought.

References

Abatzoglou, J.T., 2013. Development of gridded surface meteorological data for ecological applications and modelling. International Journal of Climatology. 33, 121-131. https://doi.org/10.1002/joc.3413

Ali, I., Cawkwell, F., Dwyer, E., Barrett, B., Green, S., 2016. Satellite remote sensing of grasslands: from observation to management. Journal of Plant Ecology. 9 (6), 649–671. https://doi.org/10.1093/jpe/rtw005

Arredondo, T., Garcia-Moya, E., Huber-Sannwald, E., Loescher, H., Delgado-Balbuana, J., Luna-Luna, M., 2016. Drought manipulation and its direct and legacy effects on productivity of a monodominant and mixed-species semi-arid grassland. Agricultural and Forest Meteorology. 223, 132-140. https://doi.org/10.1016/j.agrformet.2016.03.011

Brunsdon, C. and Chen, H. (2014). GISTools: Some further GIS capabilities for R. R package version 0.7-4. https://CRAN.R-project.org/package=GISTools

Burke, I., Lauenroth, W. 2008. The shortgrass steppe: the region and research sites. ISBN-13: 9780195135824. DOI: 10.1093/oso/9780195135824.001.0001

Churchill, A., Zhang, H., Fuller, K., Amiji, B., Anderson, I., Barton, C., Carrillo, Y., Catunda, K., Chandregowda, M., Igwenagu, C., Jacob, V., Kim, G., Macdonald,

C., Medlyn, B., Moore, B., Pendall, E., Plett, J., Post, A., Powell, J., Tissue, D., Tjoelker, M., Power, S., 2022. Pastures and Climate Extremes: Impacts of Cool Season Warming and Drought on the Productivity of Key Pasture Species in a Field Experiment. Frontiers in Plant Science, 13.

Craine, J. M., Ocheltree, T. W., Nippert, J. B., Towne, E. G., Skibbe, A. M., Kembel, S. W., & Fargione, J. E., 2013. Global diversity of drought tolerance and grassland climate-change resilience. Nature Climate Change. 3 (1), 63-67. doi:http://dx.doi.org/10.1038/nclimate1634

Fang, X., and J. Wu. 2022. Causes of overgrazing in Inner Mongolian grasslands: Searching for deep leverage points of intervention. Ecology and Society. 27(1), 8. https://doi.org/10.5751/ES-12878-270108

Gao, Y., Solórzano, J.V., Quevedo, A., Loya-Carrillo, J.O., 2021. How BFAST Trend and Seasonal Model Components Affect Disturbance Detection in Tropical Dry Forest and Temperate Forest. Remote Sensing. 13, 2033. https://doi.org/10.3390/rs13112033

Gao, Y., Solórzano, J.V., Quevedo, A., Loya-Carrillo, J.O., 2021. How BFAST Trend and Seasonal Model Components Affect Disturbance Detection in Tropical Dry Forest and Temperate Forest. Remote Sensing. 13, 2033. https://doi.org/10.3390/rs13112033

Garnier, S., Ross, N., Rudis, R., Camargo, A., Sciaini, M., and Scherer., C. (2021). Rvision - Colorblind-Friendly Color Maps for R. R package version 0.6.2.

Garnier, S., Ross, N., Rudis, R., Camargo, A., Sciaini, M., and Scherer., C. (2021). Rvision - Colorblind-Friendly Color Maps for R. R package version 0.4.0.

Goward, S., Arvidson, T., Williams, D., Faundeen, J., Irons., J., Franks., 2006. Historical record of Landsat global coverage. Photogrammetric Engineering and Remote Sensing. 72 (10). 1155-1169. https://doi.org/10.14358/PERS.72.10.1155

Guenang, G., Kamga, M., 2014. Computation of the Standardized Precipitation Index (SPI) and Its Use to Assess Drought Occurrences in Cameroon over Recent Decades. Journal of Applied Meteorology and Climatology. 53 (10), 2310-2324. https://doi.org/10.1175/JAMC-D-14-0032.1

Haddad, N., Tilman, D., Knops, J., 2002. Long-term oscillations in grassland productivity induced by drought. Natural Sciences. 5 (1), 110-120. https://doi.org/10.1046/j.1461-0248.2002.00293.x

Hijmans, R. (2022). raster: Geographic Data Analysis and Modeling. R package version 3.5-15. https://CRAN.R-project.org/package=raster

Hoagland, B., 2000. The Vegetation of Oklahoma: A Classification for Landscape Mapping and Conservation Planning. The Southwestern Naturalist. 45 (4), 385-420. https://doi.org/10.2307/3672589

Hua, L., Wang, H., Sui, H., Wardlow, B., Hayes, M., Wang, J., 2019. Mapping the Spatial-Temporal Dynamics of Vegetation Response Lag to Drought in a Semi-Arid Region. Remote Sensing. 11, 1873. https://doi.org/10.3390/rs11161873

Hyndman R, Athanasopoulos G, Bergmeir C, Caceres G, Chhay L, O'Hara-Wild M, Petropoulos F, Razbash S, Wang E, Yasmeen, F., 2021. forecast: Forecasting functions for time series and linear models. R package version 8.15, https://pkg.robjhyndman.com/forecast/.

Hyndman, RJ., Khandakar, Y., 2008. Automatic time series forecasting: the forecast package for R. Journal of Statistical Software, 26 (3), 1-22. https://www.jstatsoft.org/article/view/v027i03.

Ji, L., Peters, A., 2006. Performance evaluation of spectral vegetation indices using a statistical sensitivity function. Remote sensing of Environment. 1 (15), 59-65. https://doi.org/10.1016/j.rse.2006.07.010

Keersmaecker, W., Lhermitte, S., Honnay, O., Farifteh, Somers, B., Copping, P., 2014. How to measure ecosystem stability? An evaluation of the reliability of stability

metrics based on remote sensing time series across the major global ecosystems. Global Change Biology. 20 (7), 2149-2161. https://doi.org/10.1111/gcb.12495

Keersmaecker, W., Lhermitte, S., Tits, L., Honnay, O., Somers, B., Copping, P., 2015. A model quantifying global vegetation resistance and resilience to short-term climate anomalies and their relationship with vegetation cover. Global Change Biology. 24 (5), 539-548. DOI: 10.1111/geb.12279

Keyentash, J., and National Center for Atmospheric Research Staff (Eds). Last modified 07 Aug 2018. The Climate Data Guide: Standardized Precipitation Index (SPI). Retrieved from https://climatedataguide.ucar.edu/climate-data/standardized-precipitation-index-spi

Knapp, A., Beier, C., Briske, D., Classen, A., Luo, Y., Reichstein, M., Smith, M., Smith, S., Bell, J., Fay, P., Heisler, J., Leavitt, S., Sherry, R., Smith, B., Weng, E., 2008. Consequences of More Extreme Precipitation Regimes for Terrestrial Ecosystems. BioScience. 58 (9), 811–821, https://doi.org/10.1641/B580908

Knapp, A., Chen, A., Griffin-Nolan, R., Baur, L., Carroll, C., Gray, J., Hoffman, A., Li, X., Post, A., Slette, I., Collins, S., Luo, Y., Smith, M., 2020. Resolving the Dust Bowl paradox of grassland responses to extreme drought. PNAS. 117 (36), 22249-22255. https://doi.org/10.1073/pnas.1922030117

Lark, T., Mualler, R., Johnson, D., Gibbs, H., 2017. Measuring land-use and land-cover change using the U.S. department of agriculture's cropland data layer: Cautions and recommendations. International Journal of Applied Earth Observation and Geoinformation. 62, 24-235. https://doi.org/10.1016/j.jag.2017.06.007

Lemon, J. (2006) Plotrix: a package in the red light district of R. R-News, 6(4): 8-12.

Liu, F., Liu, H., Xu, C., Zhu, X., He, W., Qi, Y., 2021. Remotely sensed birch forest resilience against climate change in the northern China forest-steppe ecotone. Ecological Indicators. 125: 107526. https://doi.org/10.1016/j.ecolind.2021.107526

Luo, W., Griffin-Nolan, R. J., Ma, W., Liu, B., Zuo, X., Xu, C., Yu, Q., Luo, Y., Mariotte, P., Smith, M. D., Collins, S. L., Knapp, A. K., Wang, Z., and Han, X., 2021. Plant traits and soil fertility mediate productivity losses under extreme drought in C_3 grasslands. Ecology. 102 (10). https://doi.org/10.1002/ecy.3465

Ma, Z., Liu, H., Mi, Z. Zhang, Z., Wang, Y., Xu, W., Jiang, L., 2017. Climate warming reduces the temporal stability of plant community biomass production. Nature Communications. 8, 15378. https://doi.org/10.1038/ncomms15378

Mackie, K.A, Zeiter, M., Bloor, J.M.G., Stampfli, A., 2019. Plant functional groups mediate drought resistance and recovery in a multisite grassland

experiment. Journal of Ecology. 107: 937– 949. https://doi.org/10.1111/1365-2745.13102

Mariotte, P., Vandenberghe, C., Kardol, P., Hagedorn, F. and Buttler, A., 2013. Subordinate plant species enhance community resistance against drought in semi-natural grasslands. Journal of Ecology. 101: 763-773. https://doi.org/10.1111/1365-2745.12064

Masek, J.G., Vermote, E.F., Saleous, N., Wolfe, R., Hall, F.G., Huemmrich, F., Gao, F., Kutler, J., and Lim, T.K. (2006). A Landsat surface reflectance data set for North America, 1990-100, IEEE Geoscience and Remote Sensing Letters. 3:68-72.

Mesonet. Record August Puts Exclamation Point on Hottest Oklahoma Summer. Date Unknown.https://www.mesonet.org/index.php/news/article/record_august_puts_exclamation_point_on_hottest_oklahoma_summer. Accessed Oct 22, 2021.

Munson, S., Long, A., 2017. Climate drives shifts in grass reproductive phenology across the western USA. New Phytologist. 13:1945-1955. https://doi.org/10.1111/nph.14327

Oklahoma Climatological Survey. Date Unknown. The Climate of Cimarron County. http://xocs.mesonet.us/county_climate/Products/County_Climatologies/archive/county_climate_cimarron.pdf. Accessed Oct. 23. 2021.

Lionel Henry and Hadley Wickham (2020). purrr: Functional Programming Tools. R package version 0.3.4. https://CRAN.R-project.org/package=purrr

R Core Team (2021). R: A language and environment for statistical computing. R Foundation for Statistical Computing, Vienna, Austria. URL https://www.R-project.org/

Reinermann, S., Asam, S., Kuenzer, C., 2020. Remote Sensing of Grassland Production and Management-A Review. Remote Sensing. 12. 1949. doi:10.3390/rs12121949www.mdpi.com/journal/remotesensing

Robinson, N.P., B.W. Allred, W.K. Smith, M.O. Jones, A. Moreno, T.A. Erickson, D.E. Naugle, and S.W. Running. 2018. Terrestrial primary production for the conterminous United States derived from Landsat 30 m and MODIS 250 m. Remote Sensing in Ecology and Conservation. https://doi.org/10.1002/rse2.74

Rutledge, R., Basore, B., Mulholland. R., 1976. Ecological stability: An information theory viewpoint. Journal of Theoretical Biology, 57 (2), 355-371. https://doi.org/10.1016/0022-5193(76)90007-2

Souther S, Loeser M, Crews TE, Sisk T., 2020. Drought exacerbates negative consequences of high-intensity cattle grazing in a semiarid grassland. Ecol Appl. 30 (3). https://doi.org/10.1002/eap.2048

Southworth, J. & Muir, C., 2021. Specialty Grand Challenge: Remote Sensing Time Series Analysis. Frontiers in Remote Sensing. 2. https://doi.org/10.3389/frsen.2021.770431

Tebbs, E.J., Rowland, C.S., Smart, S.M., Maskell, L.C., Norton, L.R., 2017. Regional-Scale High Spatial Resolution Mapping of Aboveground Net Primary Productivity (ANPP) from Field Survey and Landsat Data: A Case Study for the Country of Wales. Remote Sensing. 9, 801. https://doi.org/10.3390/rs9080801

Tilman, D., Downing, J., 1994. Biodiversity and stability in grasslands. Nature. 367, 363–365. https://doi.org/10.1038/367363a0

Tillman, D., Haddi, E., 1992. Drought and biodiversity in grasslands. Oecologia. 89 (2) 257-264. https://doi.org/10.1007/BF00317226

Tilman, D., Reich, P. & Knops, J., 2006. Biodiversity and ecosystem stability in a decade-long grassland experiment. Nature. 441, 629–632. https://doi.org/10.1038/nature04742

USDA, 2019. 2019 Oklahoma Agricultural Statistics. Accessed 3/26/2021. https://www.nass.usda.gov/Statistics_by_State/Oklahoma/Publications/Annual_Statistical_Bulletin/ok-bulletin-2019.pdf

USDA National Agricultural Statistics Service Cropland Data Layer. 2006-2020. Published crop-specific data layer.

Vadjunec, J., Boardman, A., Fagin, T., Larson, M., Kedron, P., Brian, B., 2021. Footprints from the Dust Bowl: Using Historical Geographic Information Systems to Explore Land and Resource Access, Use, and Survivability in "No Man's Land," Cimarron County, Oklahoma, Annals of the American Association of Geographers. 111:7, 1906-1930. DOI: 10.1080/24694452.2020.1867497

Van Ruijven, J. and Berendse, F., 2010. Diversity enhances community recovery, but not resistance, after drought. Journal of Ecology, 98: 81-86. https://doi.org/10.1111/j.1365-2745.2009.01603.x

Verbesselt J, Hyndman R, Newnham G, Culvenor D., 2010. Detecting Trend and Seasonal Changes in Satellite Image Time Series. Remote Sensing of Environment, 114 (1), 106–115. doi: 10.1016/j.rse.2009.08.014.

Verbesselt J, Hyndman R, Zeileis A, Culvenor D., 2010. Phenological Change Detection while Accounting for Abrupt and Gradual Trends in Satellite Image Time

Series. Remote Sensing of Environment. 114 (12), 2970–2980. doi: 10.1016/j.rse.2010.08.003

Verbesselt, J., Zeileis, A., Herold., M., 2012. Near real-time disturbance detection using satellite image time series. Remote Sensing of Environment. 123, 98-108. https://doi.org/10.1016/j.rse.2012.02.022

Vicca, S., Balzarolo, M., Filella, I., Filella, I., Granier, A., Herbst, M., Knohl, A., Longdoz., B., Mund, M., Nagy, Z., Pinter, K., Verbesselt, J., Verger, A., Zeileis, A., Zhang, C., Penuelas, 2016. Remotely sensed detection of effects of extreme droughts on gross primary production. Scientific Reports. 6, 28269. https://doi.org/10.1038/srep28269

Vogel., A., Scherer-Lorenzen, M., Weigelt, A., 2012. Grassland Resistance and Resilience after Drought Depends on Management Intensity and Species Richness. PLoS One. 7 (5). https://doi.org/10.1371/journal.pone.0036992

Wang, H., Pan Y., Chen, Y., 2017. Comparison of three drought indices and their evolutionary characteristics in the arid region of northwestern China. Atmospheric Science Letters. 18 (3), 13-139. https://doi.org/10.1002/asl.735

Wang, Q., Yang, Y., Liu, Y. Tong, L., Zhang, Q., Li., J., 2019. Assessing the Impacts of Drought on Grassland Net Primary Production at the Global Scale. Scientific Reports. 9, 14041

Weltzin, J., Loik, M., Schwinning, S., Williams, D., Fay, P., Haddad, B., Harte, J., Huxman, T., Knapp, A., Lin, G., Pockman, W., Shaw, R., Small, E., Smith, M., Smith, S., Tissue, D., Zak, J., 2003. Assessing the Response of Terrestrial Ecosystems to Potential Changes in Precipitation. BioScience. 53 (10) 941–952. https://doi.org/10.1641/0006-3568(2003)053[0941:ATROTE]2.0.CO;2

White, H.J., Gaul, W., Sadykova, D., León-Sánchez, L., Caplat, P., Emmerson, M.C., Yearsley, J.M., 2020. Quantifying large-scale ecosystem stability with remote sensing data. Remote Sensing in Ecology and Conservation. 6: 354-365. https://doi.org/10.1002/rse2.148

Wilcox, K., Koerner, S., Hoover, D., Borkenhagen, A., Burkepile, D., Collins, S., Hoffman, A., Kirkman, K., Knapp, A., Strydom, T., Thompson, D., Smith., M., 2020. Ecology. Rapid recovery of ecosystem function following extreme drought in a South African savanna grassland. 101 (4).

Witwicki, D. L., S. M. Munson, and D. P. Thoma., 2016. Effects of climate and water balance across grasslands of varying C3 and C4 grass cover. Ecosphere. 7 (11). DOI: 10.1002/ECS2.1577

Xu, C., Ke, Y., Zhou, W., Luo, W., Ma, W., Song, L., Smith, M., Hoover, D., Wilcox, K., Fu, W., Zhang, W.,Yu, Q., 2021. Resistance and resilience of a semi-arid

grassland to multi-year extreme drought. Ecological Indicators. 131. https://doi.org/10.1016/j.ecolind.2021.108139

Zhang, L, Wylie, B., Gilmanov, T., Tieszen, L., Howard, D., 2011. Upscaling carbon fluxes over the Great Plains grasslands: Sinks and sources. Journal of Geophysical Research: Biogeosciences. 116 (1). https://doi.org/10.1029/2010JG001504

Zhang, L., Xiao, J., Zhou, Y., Zheng, Y., Li, J., and Xiao, H., 2016. Drought events and their effects on vegetation productivity in China. Ecosphere. 7 (12). https://doi.org/10.1002/ecs2.1591

Zhong, S., Sun, Z., Di, L., 2021. Characteristics of vegetation response to drought in the CONUS based on long-term remote sensing and meteorological data. Ecological Indicators. 127: 107767. https://doi.org/10.1016/j.ecolind.2021.107767

Zhou, S., Zhang, Y., Williams, A., Gentine, P., 2019. Projected increases in intensity, frequency, and terrestrial carbon costs of compound drought and aridity events. 5. (1).

Table 1. Mean values of SPI, EVI, and GPP for both kept and discarded grassland pixel values. These values show similarity between both kept and discarded pixels, indicating LULC change was not likely a major factor influencing our results.

SPI mean:	-0.16815	EVI mean:	0.167525	GPP mean:	169.99442
Discarded SPI mean:	-0.12263	Discarded EVI mean:	0.151180	Discarded GPP mean:	194.12666

Table 2. Seasons with mean SPI values above one and below negative one, indicating a drought or pluvial event with precipitation amounts one or more standard deviations from the long-term mean. Out of 64 total seasons in the study timeframe, 27 (42.2%) were drought or pluvial periods.

	Winter	**Spring**	**Summer**	**Fall**
Occurrences of SPI values above 1	2	4	4	3
Occurrences of SPI values below 1	3	4	4	3

Table 3. Average intensity of each season's drought events. Summer droughts exhibited by far the least intensity. Fall is shown to be the season hit by the most intense droughts, while those occurring during spring and winter were of approximately the same magnitude.

	Winter	**Spring**	**Summer**	**Fall**
Mean SPI of each season's droughts	-1.64	-1.65	-1.14	-1.70

Table 4. Average intensity of each season's SPI. Fall stands out as having by far the lowest average SPI from 2005-2020, approximately five times more intense than the second lowest average SPI. This, along with values from table three, suggest October-December are the months most effected by precipitation deficits from 2005-2020.

	Winter	**Spring**	**Summer**	**Fall**
Average SPI for each season	-0.014	-0.053	-0.029	-0.261

Table 5. Results from linear regression between each metric's mean values for each pixel. The relationships between SPI and vegetation structure and function are moderately strong, with high significance. However, the relationship between vegetation structure and vegetation function is quite weak, albeit significant.

	R^2	p-value
SPI ~ EVI	0.5879	< 2.2e-16
SPI ~ GPP	0.5868	< 2.2e-16
EVI ~ GPP	0.1381	< 2.2e-16

Table 6. Mean coefficient of variation for each season and overall timeframe. SPIcv shows much more variation for every season and over the entire timeframe, when compared to EVIcv and GPPcv. According to CV, vegetation structure presents much less variation over time than does vegetation function.

	Winter	**Spring**	**Summer**	**Fall**	**Overall**
SPI	123.3001	116.5121	116.381	110.8467	117.0814
EVI	21.39526	32.88325	24.5088	18.58392	40.88374
GPP	28.86614	47.91747	29.54114	29.35662	87.97059

Table 7. Results from linear regression between the coefficient of variation of vegetation structure (EVI), function (GPP), and drought (SPI). Very weak, but significant relationships are shown between each variable.

	R^2	p-value
SPIcv ~ EVIcv	0.007	2.2e -16
SPIcv ~ GPPcv	0.038	2.2e -16
EVIcv ~ GPPcv	0.1968	2.2e -16

Figure 1. Location of Cimarron County, Oklahoma. The county is situated in the Southern Great Plains at the far western extent of the Oklahoma panhandle, bordered by Colorado and Kansas to the North, New Mexico to the West, and Texas to the South.

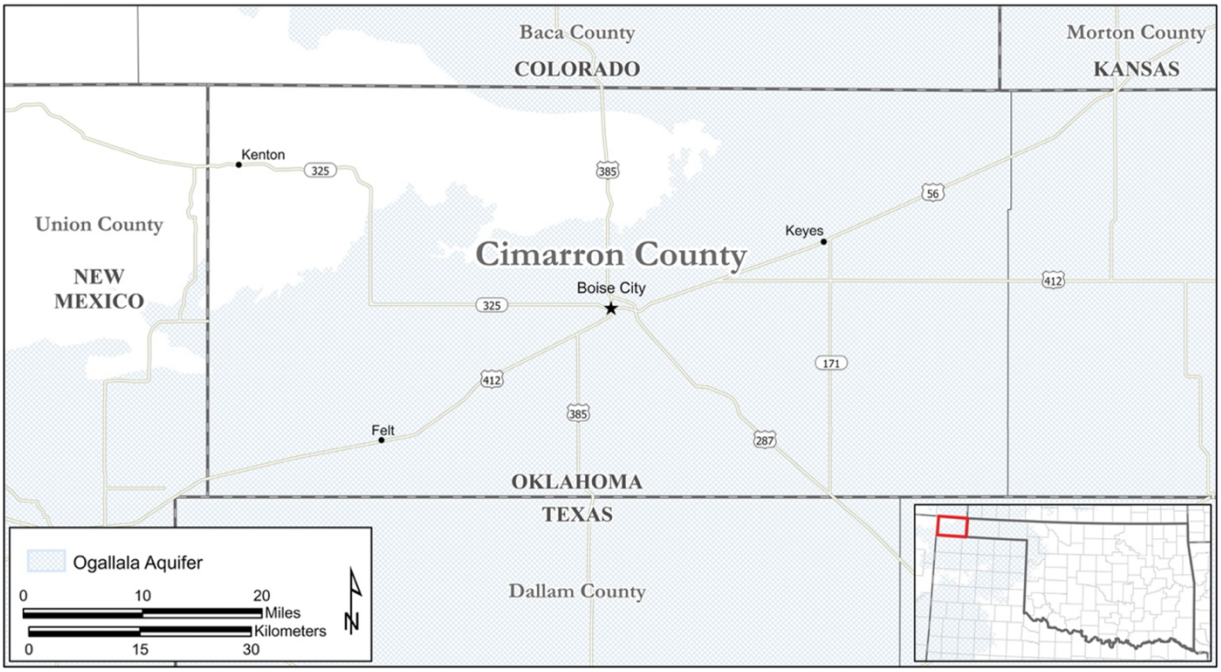

Vadjunec, J., et al. 2021

Figure 2. Mean monthly minimum, maximum, and average temperatures (A) from 1995-2010 and mean monthly precipitation (B) for Boise City from 1995-2020. The highest average temperatures occur in July, while the most precipitation tends to fall in August. It is not uncommon for the county to experience multiple consecutive months with less than one centimeter of precipitation.

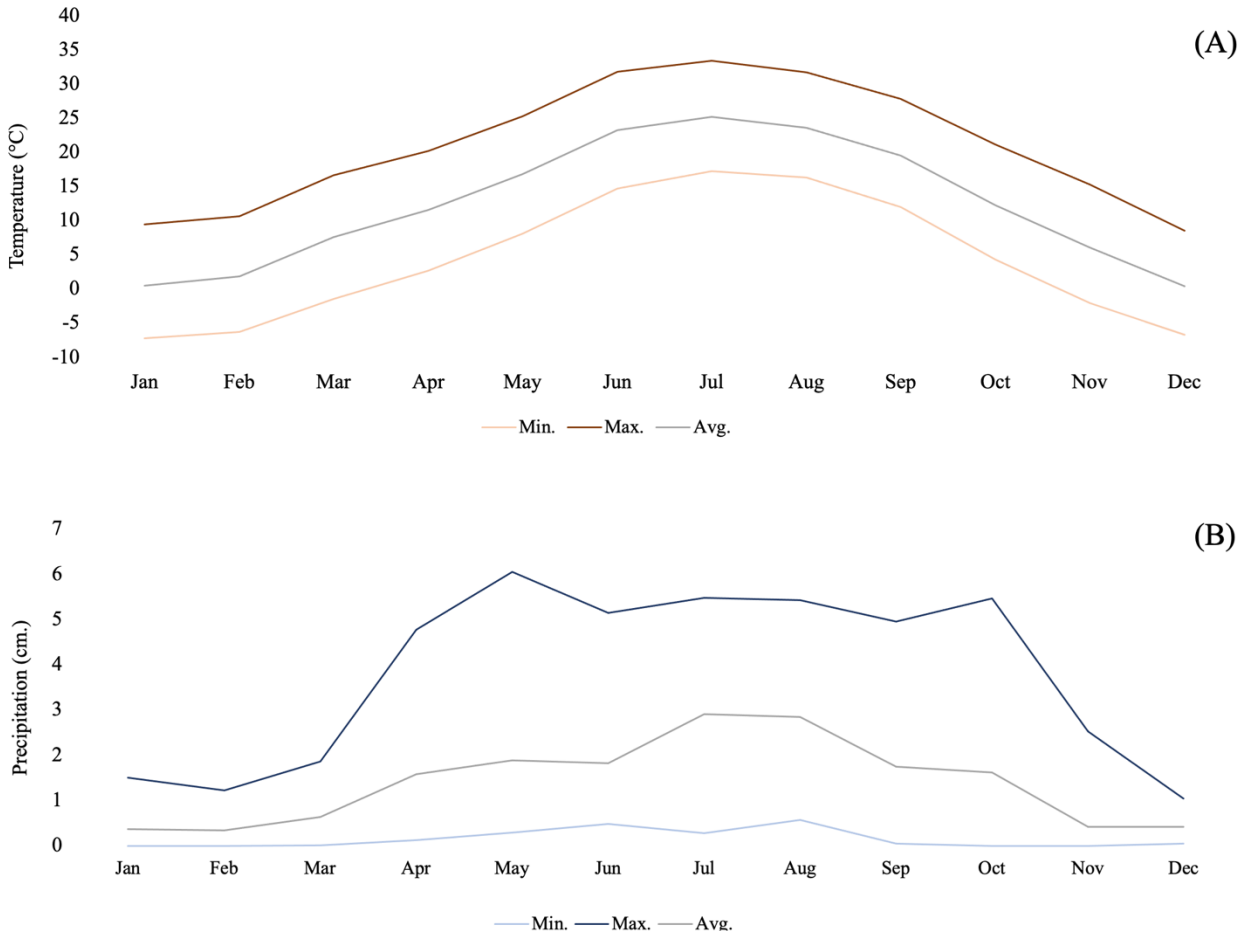

Figure 3. Land cover change of the three most common LULC types in Cimarron County from 2006-2020. There is a steady and substantial decrease in grassland area from 2006-2020, with slight increases in shrublands. Winter wheat shows a steady increase for the first 10 years, then continuously declines through 2020, though sorghum appears to be replacing winter wheat during this decline.

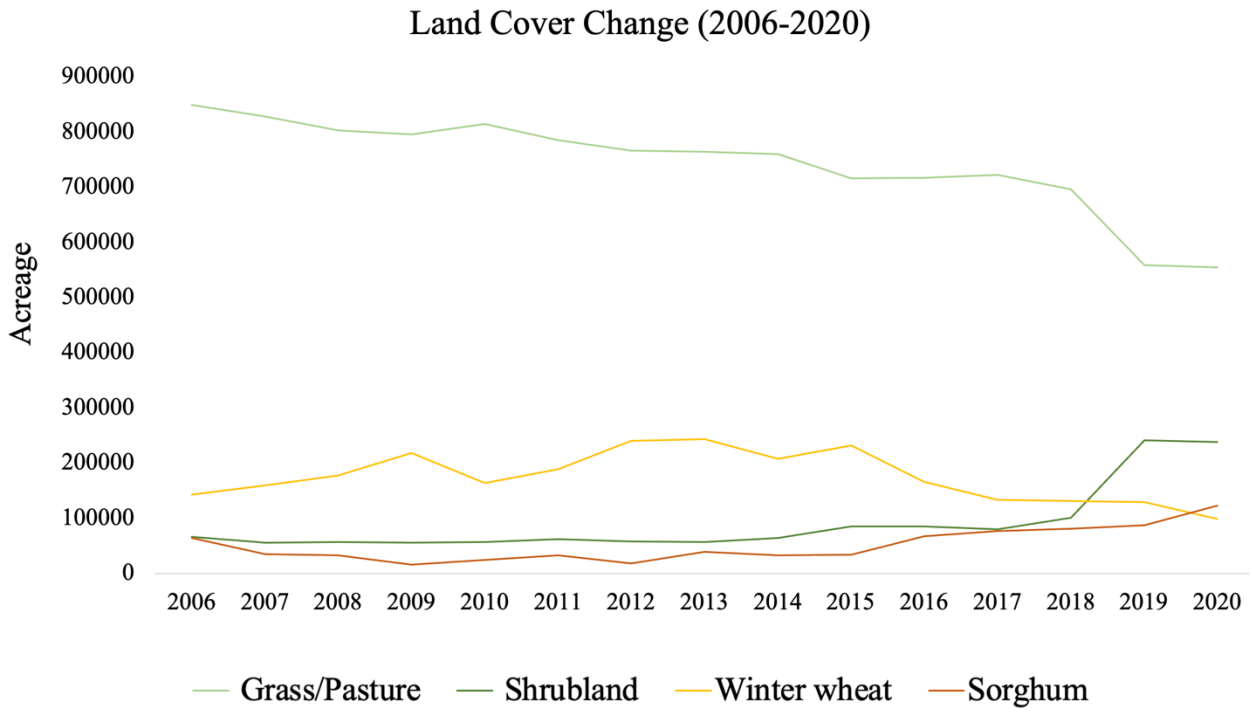

Figure 4. Visualization of the calculation and interpretation of the Standardized Precipitation Index. The bell curve is composed of precipitation values taken from a long-term dataset of the specified study area. The values on the Y-axis indicate the probability of a precipitation event along the corresponding point of the curve. The values on the bottom X-axis indicate SPI values and their corresponding "dryness", denoting how many standard deviations the amount of precipitation is above or below the long-term mean. The percentages between the dashed lines indicate the probability SPI will fall within that range. An SPI of zero would indicate the mean precipitation for the input precipitation dataset.

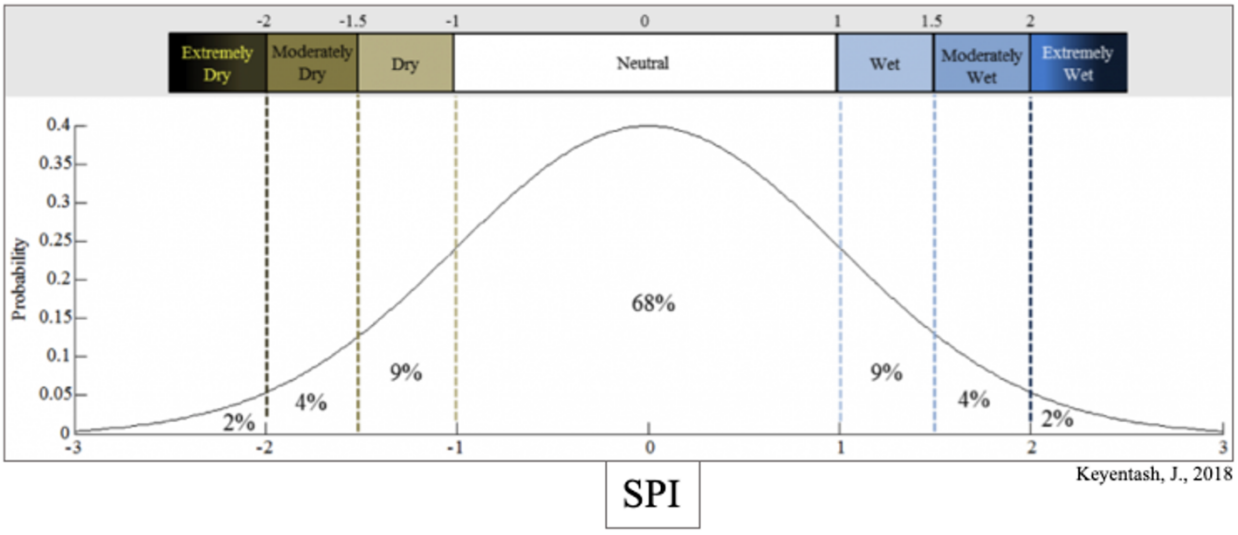

Figure 5. Process of upscaling and clipping Cimarron County to grasslands. Plot A shows the original SPI image for Summer 2010 (year and season chosen at random for this example), with a spatial resolution of approximately 4,000 meters. Plot B shows the same image upscaled to a spatial resolution of 30 meters. Plot C shows the upscaled image clipped to grasslands as determined by the Cropland Data Layer from 2010.

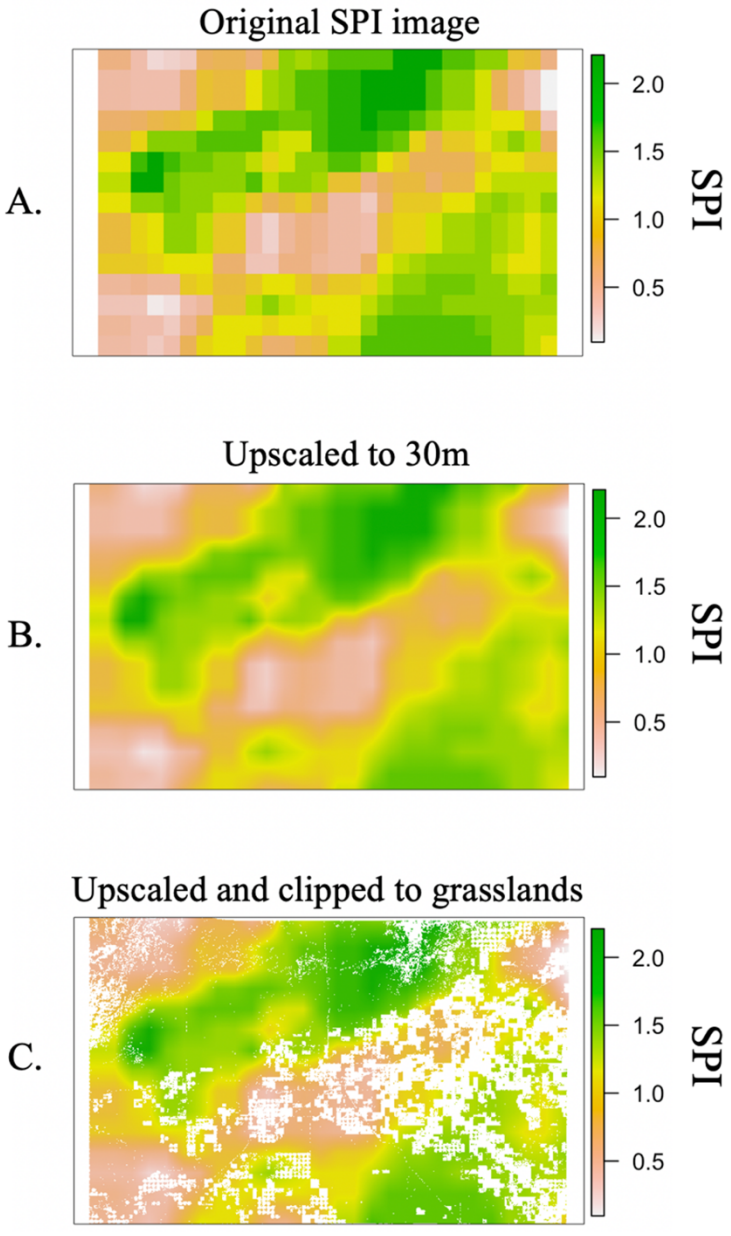

Figure 6. Red dashed lines indicate SPI thresholds of one and negative one SPI, indicating values above or below these are at least one standard deviation from the long-term mean**.** Red circles generally encapsulate time periods in which SPI values reach above or below these thresholds. While every season (64 total) are included in the plot, only winter and summer are included on the X-axis due to limitations on space.

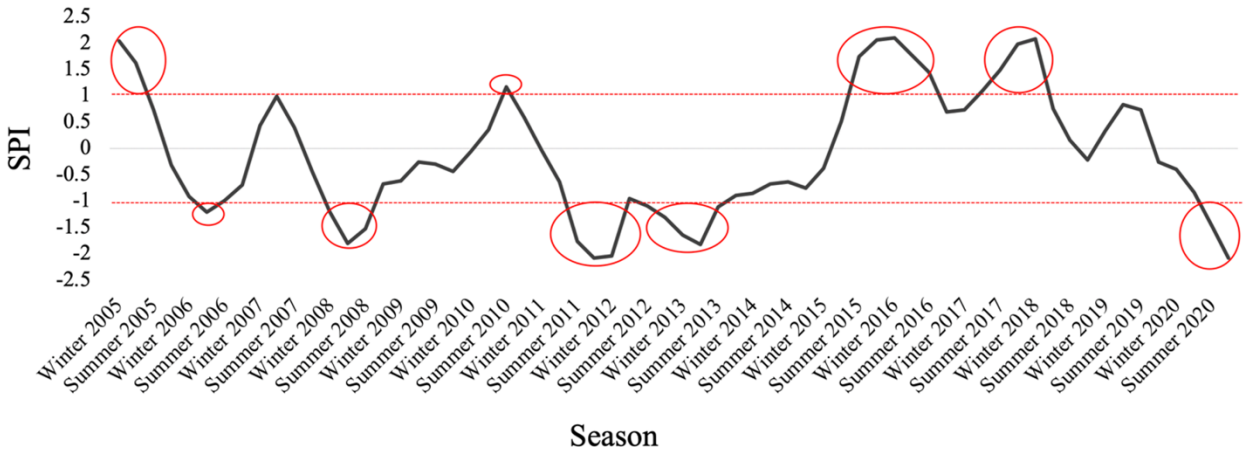

Figure 7. Trend and breakpoint timing for each time series (A: SPI; B: EVI; C: GPP). Solid black lines indicate the input temporal data for each metric. Solid blue lines show the trendlines drawn along the input data for each segment between breakpoints. Vertical dashed black lines indicate the breakpoints within each time series. Confidence intervals for each breakpoint are colored in red. EVI and GPP time series each have three breakpoints while SPI has four. The lack of a fourth breakpoint in EVI and SPI data may indicate stability under the effects of intense drought. All three confidence intervals for EVI and GPP overlap with those of SPI, apart from the third GPP breakpoint which occurred one season prior to the lower bound of the corresponding SPI breakpoint. The timing of the structural breaks indicate synchronicity between drought, vegetation structure, and vegetation function.

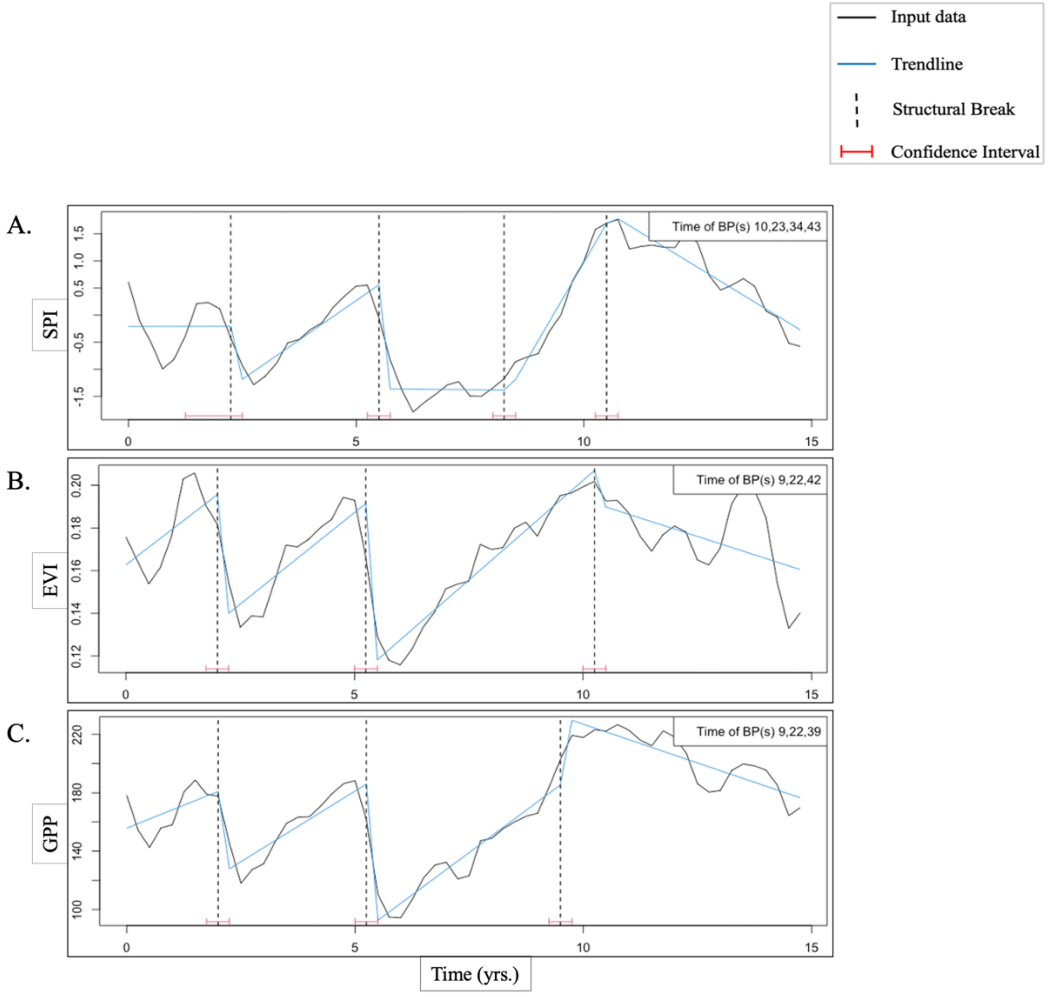

Figure 8. Coefficient of variation of each season for SPI, EVI, and GPP from 2005-2020. Coefficient of variation values are indicated on the Y-axis of each plot. Each plot is composed of CV values calculated from 16 images (one for each season across a 16-year timeframe).

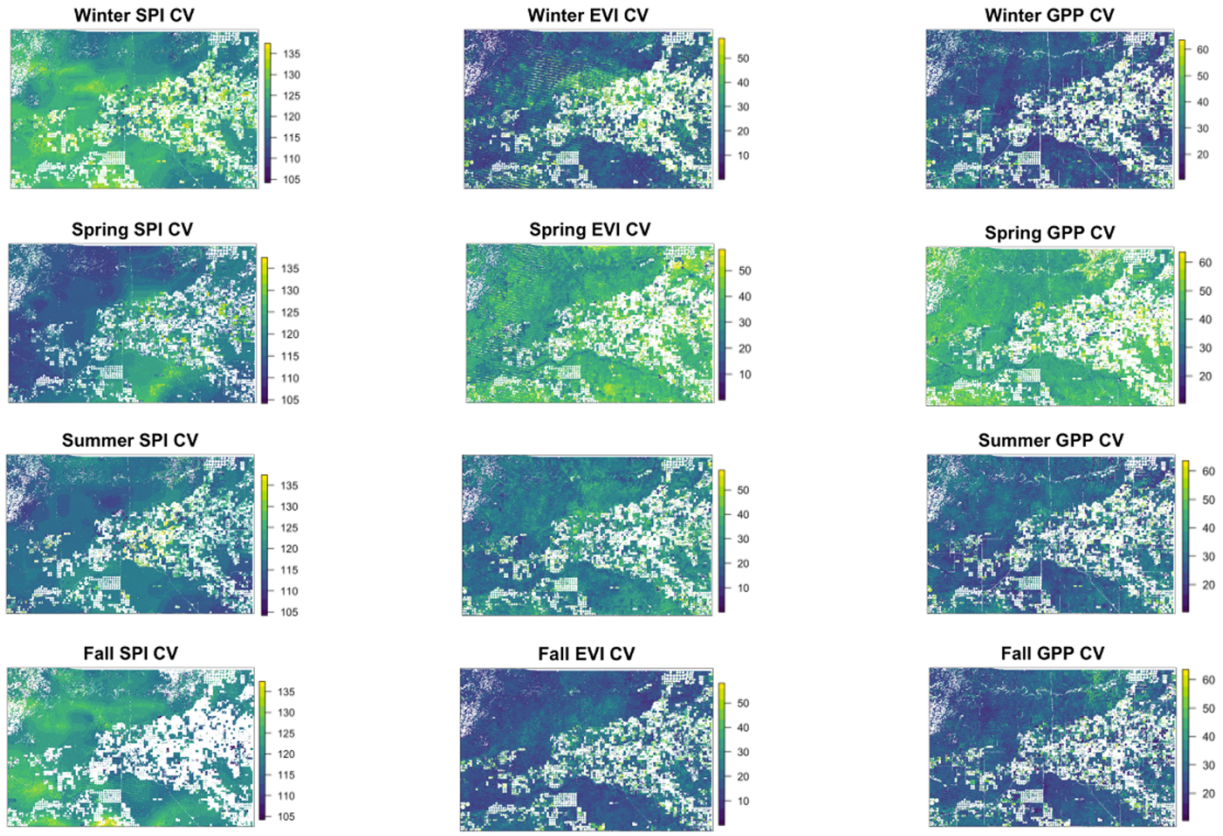

Figure 9. Coefficient of variation for SPI, EVI, and GPP across the full 16-year timeframe (64 seasons). Coefficient of variation values are indicated on the Y-axis of each plot. SPI shows markedly more variation than EVI and GPP across the entire county. While SPIcv seems to be generally bound to a smaller range of variation, EVIcv and GPPcv show more heterogeneity across the landscape.

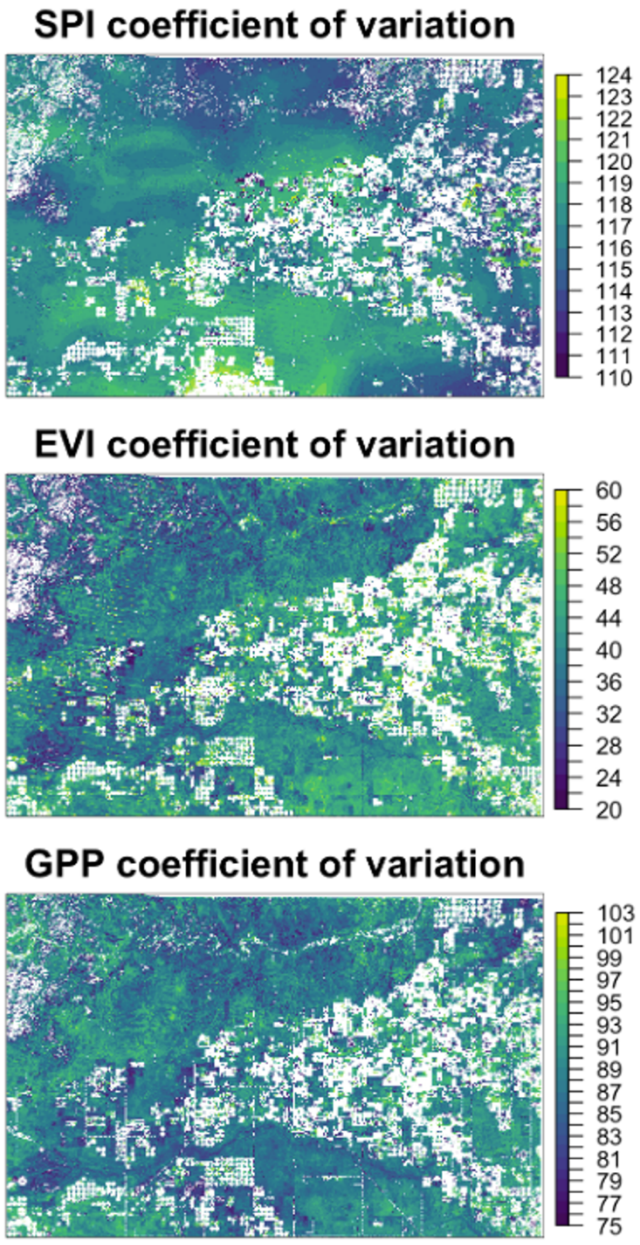

Figure 10. The histograms below show the distribution of coefficient of variation values for SPI (drought), EVI (veg. structure), and GPP (veg. function). These results show a much higher and more narrow distribution of SPI variation, indicating high fluctuation, but relative uniformity across the county for the 16-year period. Vegetation structure indicated the lowest variation and widest range.